Available online at www.sciencedirect.com
SCIENCE DIRECT®
Diamond and Related Materials 12 (2003) 1346–1356
DIAMOND AND RELATED MATERIALS
www.elsevier.com/locate/diamond

Number density and temperature of acetylene in hot-filament and arc-jet activated CH_4/H_2 gas mixtures measured using diode laser cavity ring-down absorption spectroscopy

Jonathan B. Wills[a], Michael N.R. Ashfold[a], Andrew J. Orr-Ewing[a,*], Yuri A. Mankelevich[b], Nikolay V. Suetin[b]

[a]*School of Chemistry, University of Bristol, Cantock's Close, Bristol BS8 1TS, UK*
[b]*Nuclear Physics Institute, Moscow State University, 119899 Moscow, Russia*

Received 4 October 2002; received in revised form 1 February 2003; accepted 8 February 2003

Abstract

Continuous-wave cavity ring-down spectroscopy (CW-CRDS) with an external cavity diode laser has been used to make diagnostic measurements of acetylene absorption in hot-filament and DC-arc plasma jet reactors operating with 1% CH_4 in H_2 and $\leq 0.8\%$ CH_4/H_2 in excess Ar, respectively, and used for diamond chemical vapour deposition. The acetylene was widely distributed throughout the reactor, extending well beyond the regions of highest thermal activation as a result of diffusion processes. The average acetylene concentration was determined as $(2.9 \pm 0.6) \times 10^{13}$ molecules cm^{-3} in the hot filament reactor and $(1.2 \pm 0.2) \times 10^{14}$ molecules cm^{-3} in the DC arc jet reactor, accounting for $\sim 1.7\%$ and 40% of the total C budget in the respective cases. The average acetylene gas temperature along the viewing column was 550 ± 150 K in both environments. Variations in the concentration and temperature of acetylene with the gas feed composition and input power processing conditions for the two reactors are presented. The experiments demonstrate the effectiveness of near-IR diode laser CRDS as a probe of highly luminous environments.

Keywords: Continuous-wave cavity ring-down spectroscopy; Diamond chemical vapour deposition; Acetylene distribution

1. Introduction

Chemical vapour deposition (CVD) is now a well-established technique for growth of polycrystalline diamond films. Such materials are finding ever-increasing technological uses, for example as wear-resistant coatings and infra-red windows, and have an expanding range of electronic and electrochemical applications [1,2]. Most diamond CVD involves activation of a dilute hydrocarbon/H_2 mixture (e.g. 1% CH_4 in H_2) at a pressure of a few tens of Torr, and subsequent growth on the chosen substrate material maintained at the necessary elevated process temperature (typically ~ 800 °C) [3]. Essential to such growth processes is the formation of H atoms in the reaction mixture. In a hot-filament (HF) reactor, H atoms are created by thermal dissociation at the filament surface, whereas in plasma devices H atoms are formed by a combination of thermal dissociation of H_2 and dissociation via collisions with high-energy electrons, ions and metastables in the plasma. These H atoms are accredited with several key growth roles. Crucially, they can react with the hydrocarbon precursors to produce carbon (C_1)-based radicals (e.g. CH_3) that adsorb onto and react with the substrate, and subsequently the growing film. C_1 radicals also react with each other to form C_2 species, one of which is acetylene. Studies of acetylene/H_2 precursor gas mixtures show very similar diamond growth properties [4] to the standard CH_4/H_2 mixtures, suggesting common intermediate species and significant inter-conversion between C_2 and C_1 compounds. As demonstrated in this paper, however, the chemical stability of acetylene in the activated gas mixture means that once formed, it can diffuse throughout the reactor, resulting

*Corresponding author. Tel.: +44-117-928-7672; fax: +44-117-925-0612.
E-mail address: a.orr-ewing@bris.ac.uk (A.J. Orr-Ewing).

0925-9635/03/$ - see front matter © 2003 Elsevier Science B.V. All rights reserved.
PII: S0925-9635(03)00085-2

in a comparatively high, steady-state abundance in colder, stagnant regions of the reaction chamber.

In conjunction with the experimental work presented here, extensive effort has been devoted to modelling of the gas-phase chemistry and transport properties in the Bristol reactors. The model of the HF reactor has evolved to the point where it gives excellent agreement with experimental measurements of concentrations and profiles of reactive species (H and CH_3, and, in the case of $NH_3/CH_4/H_2$ mixtures, NH) in the region of the reactor between the filament and the substrate [5–7]. The current study offers the opportunity for additional tests of the model further from the filament, in cooler regions of the reactor. Models of the chemistry, activation processes and flow in the DC arc jet are also being developed [8].

This paper presents results of measurements of the concentration and temperature of acetylene in both HF and DC arc jet-activated CH_4/H_2 gas mixtures using a newly developed diode laser cavity ring-down spectrometer. Variations in the acetylene concentration with operating parameters of the reactors are reported, and fractions of the total input carbon converted into C_2H_2 are derived. Data for the HF reactor are compared with the results of theoretical modelling of the gas-phase chemistry, diffusion rates and residence times of C_2H_2, and the CRDS measurements provide a critical test of the predictions from the model of absolute C_2H_2 concentrations.

2. Experimental

The hot-filament and DC arc jet reactors are capable of growing polycrystalline diamond films at respective rates of 1 and 100 μm h^{-1}. Details of the HF-CVD [9] and DC-arc jet CVD reactors [10] are given elsewhere and are summarised only briefly here. More attention is given to the optical set-up used to measure C_2H_2 concentrations, because this has not been described previously.

The HF reactor is an evacuable, six-way stainless steel cross with volume $V=6.6$ l, equipped with two micrometer-adjustable mirror-mount flanges. From the top flange of the cross, the HF (250-μm-diameter Ta wire, seven turns, ~3-mm coil diameter, 12 mm long) is mounted on a linear transfer mechanism allowing vertical translation of the filament by ≤25 mm. The HF temperature (T_{fil}, typically 2150 °C) is monitored with a two-colour optical pyrometer (Land Infrared) through a quartz window. Power is supplied to the HF from a DC power supply via feed-throughs to one side of the HF; the other end is grounded. Feed gases (1% CH_4/H_2) are delivered via mass flow controllers, premixed in a manifold and enter the chamber through a port located slightly above the HF so as to maintain an overall flow rate of 100 sccm and a chamber pressure of 20 Torr. Experiments described here were performed without a substrate present.

The DC-arc plasma jet (Aeroplasma Corp) reactor consists of a custom-made, hollow-walled (for water cooling) cylindrical stainless steel chamber with several quartz viewing ports and two extended arms perpendicular to the cylinder axis, on which micrometer-adjustable mirror mounts are attached. At one end of the cylinder, the chamber is extended by edge-welded bellows to a terminating flange, through which the 28-mm-diameter molybdenum substrate is mounted on a long, water-cooled (closed water system, chilled to 11 °C, pumped to 9 bar) steel tube. This assembly allows the substrate position in the chamber to be translated (by up to ±20 mm) in three dimensions. At the other end of the cylinder, the torch head assembly is mounted on a large copper flange. The twin torch consists of an N-torch, through which the primary flow of Ar is mixed with a secondary spiral stream of Ar/H_2. Perpendicular to the N-torch is the smaller P-torch, through which a further stream of Ar is added to the jet. Total gas throughputs are typically 10 slm of Ar in the primary flow through the N-torch, with a further 0.75 slm through the P-torch and a mix of 1.4 slm $Ar/1.8$ slm H_2 in the secondary N-torch flow. The total pressure in the reactor is maintained at 50 Torr. The plasma is initiated by a DC arc across the torch nozzles, with typical power supplied being 5–6 kW, though the arc-jet is designed to operate at up to 10 kW. Methane (usually 60 sccm, i.e. 3.3% of the total flow of H_2 for optimal diamond growth, but restricted to ≤15 sccm in this study) is introduced to the H_2/Ar plasma through a circular injection ring located 100 mm downstream of the nozzle, thereby preventing amorphous carbon deposition on the nozzles.

For both CVD reactors, laser wavelengths in the region of 1.51 μm (6610 cm^{-1}) were used to probe individual rotational lines of the $\nu_1+\nu_3$ vibrational combination band of acetylene. This radiation was generated by a Littman-configuration extended-cavity diode laser (ECDL) (Sacher Lasertechnik). The optical set-up is shown schematically in Fig. 1 and is similar to that used by Romanini and co-workers [11] and Schulz and Simpson [12]. Approximately 50% of the laser probe beam was deflected off axis by an acousto-optic modulator (AOM) (Isle Optics; 80 MHz) into a single-mode fibre optic that contained an optical isolator (ThorLabs) to protect the laser from radiation reflected from the cavity mirrors. The output end of the fibre was positioned in front of one of the cavity mirrors (Layertec $R>99.97\%$) and the output light collimated using a very short-focal-length lens ($f\approx5$ mm). A second lens (HF reactor $f=50$ cm, arc jet $f=75$ cm) was used to focus the laser gently toward the centre of the cavity to encourage preferential excitation of the TEM_{00} cavity mode. In the HF reactor, the cavity axis was parallel to the long axis of the coiled filament, and in the DC arc

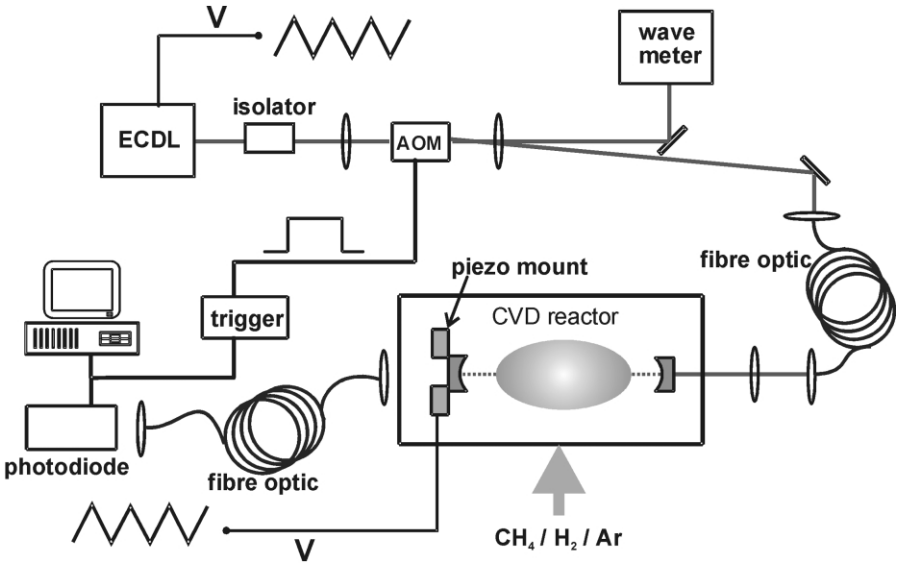

Fig. 1. A schematic diagram of the CW-CRDS spectrometer. The optical set-up was very similar for measurements in the HF and arc jet reactors. Either the laser wavelength or a piezoelectric transducer holding one cavity mirror was modulated using a triangular voltage waveform to achieve cavity excitation by the diode laser beam. Abbreviations used in the figure are: ECDL, external cavity diode laser; and AOM, acousto-optic modulator.

jet reactor, the centre lines of the cavity and gas plume crossed at 90°. The power delivered to the front mirror of the cavity was typically 250 μW. The level of laser light leaking from the cavity was continuously monitored with a fibre optic coupled to a fast-response photodiode detector (New Focus 1811-FC) positioned behind the opposing cavity mirror. A valuable feature of using a fibre optic to collect the signal is the strong discrimination against background radiation from the hot reactor because of precise directional alignment of the fibre to the probe beam. To encourage excitation of cavity modes, the laser frequency was modulated by approximately one cavity free spectral range at a rate of 100 Hz. When the laser and cavity modes passed through resonance and sufficient light built up within the cavity (as measured by the detector), the AOM was triggered to extinguish the deflected beam and the light within the cavity then decayed exponentially with rate coefficient, k, dependent on the mirror reflectivities, the length of the cavity, ℓ, and the presence of any absorbing media. Typical $1/e$ ring-down times were 8.5 μs in the HF reactor and 5 μs in the arc jet reactor. Mirror losses were quantified, and changes in rate coefficient, Δk, observed when tuning across an absorption line, were converted directly into absorbance [13], thereby enabling measurement of absolute concentrations of absorbers. Scanning the laser wavelength and measuring Δk at each frequency generated a spectrum. Data were acquired with a digital oscilloscope (LeCroy 9360) and coupled into custom LABVIEW software on a computer, where individual ring-down events were fitted to an exponential function. Those with large fit errors (caused for example by mechanical vibrations) were rejected and the measurement automatically repeated. Typically, five k values were averaged at each frequency to generate the final data points. The typical standard deviation for these final points was 1–2% of the mean k value for a data set containing no absorption features. Precise wavelength calibration was achieved using a wavemeter (Burleigh WA-1000). The laser frequency was tuned and modulated by a piezo-electric actuator within the mount of the cavity-tuning mirror of the ECDL. The modulation and scanning of the laser frequency were controlled by an analogue voltage, selected through the LABVIEW software, and interfaced via a data acquisition card (National Instruments PCI 6024E).

The frequency selection by the cavity, with free spectral range (for the HF reactor) of 238 MHz and finesse of $\sim 10^4$, severely limits the frequencies at which absorption measurements can be made across a narrow spectral feature. Typical full width at half-maximum (FWHM) values for Doppler-broadened lines of C_2H_2 are $\sim$600 MHz, which would mean that only two or three frequency points across the profile could be measured for the case of a perfectly stable cavity arrangement. In our experiments, small vibrations in the optical system due to damped rotary pumps and cooling fans have the effect of randomly dithering the cavity length, and thus changing the longitudinal mode frequencies of the cavity enough to allow most frequencies to excite the cavity at some time during each measurement period. Relying on these vibrations alone to bring the laser and cavity into resonance, without the additional 100-Hz modulation of the laser frequency, did not, however,

give sufficiently reliable scans of spectra because of the erratic behaviour of the vibrations on the timescale of each measurement. An alternative method to achieve cavity excitation at all laser frequencies is to control and dither the cavity length with a piezo-electric actuator [11]. This method was found to be less convenient than the modulation of the laser frequency, however, proving more difficult to establish stable periods of regular cavity excitation.

Modulating the laser frequency might be expected to add width to an individual absorption line. However, careful comparisons of measurements of linewidths made in this way and those employing the cavity-length dithering technique described above showed very good agreement. At the level of accuracy of the present measurements, any additional broadening introduced by periodic modulation of the laser frequency is not significant.

3. Results and discussion

Individual, isolated rotational lines of the $\nu_1+\nu_3$ vibrational combination band of C_2H_2 were selected using criteria of line strength and stability of the single-mode operation of the ECDL over the line profiles. Spectra of individual rotational lines were recorded and fitted using Gaussian functions to derive intensities and linewidths. The entire ro-vibrational absorption band was simulated using the PGOPHER [14] software and spectroscopic constants from Smith and Winn [15], and absolute integrated line strengths at required temperatures were derived from the simulations by scaling from the data at 296 K of El Hachtouki and Van der Auwera [16].

3.1. Gas temperatures

Fig. 2 shows a sample profile obtained by scanning across the R(22) rotational line of the $\nu_1+\nu_3$ band of C_2H_2 at $\nu=6603.41$ cm^{-1}, together with a best fit to the data in terms of a Gaussian lineshape. This probe transition was used to extract both temperatures and concentrations when using CH_4 in H_2 input feed gas mixtures in the HF reactor. The linewidth is dominated by Doppler broadening. The FWHM ($\Delta\nu$) of such profiles provides an effective gas temperature (T_{gas}) via the relationship:

$$\Delta\nu=\frac{\nu}{c}\left(\frac{8k_B T_{gas}\ln 2}{m}\right)^{1/2} \quad (1)$$

where m is the mass of the absorber, ν is the line centre frequency, c is the speed of light and k_B is the Boltzmann constant. The FWHM deduced for the transition shown in Fig. 2 is $\Delta\nu=0.022\pm0.003$ cm^{-1} (650 ± 90 MHz)

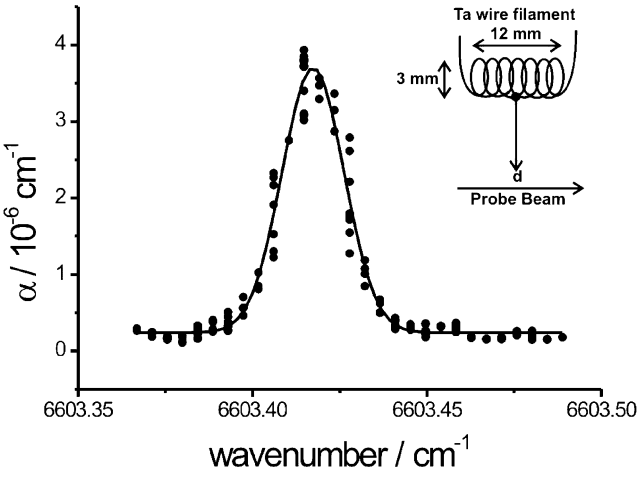

Fig. 2. An example of a typical CRDS absorption line profile: the R(22) line of the C_2H_2 $\nu_1+\nu_3$ combination band recorded in the HF reactor under diamond film growth conditions (1% CH_4 in H_2, $T_{fil}=$ 2150 °C, $p=20$ Torr, $d=3$ mm). Derivation of the vertical scale for the absorption coefficient (in units of cm^{-1}) makes the assumption that the absorber fills the entire space between the two cavity mirrors. The limited resolution of the wavemeter results in several intensity points being plotted at the same nominal wavenumber, despite frequency steps by the laser. The inset shows the dimensions of the hot filament and the arrangement of laser and filament axes.

(1σ uncertainty). Instrumental contributions to the linewidth are negligible, since the ECDL has a characteristically narrow linewidth (~4 MHz), and pressure-broadening at reactor pressures is small (as estimated from the broadening coefficient of ~4 MHz Torr^{-1} for C_2H_2 in Ar) [17]. The FWHM measured translates into an effective gas temperature $T_{gas}=550\pm150$ K. This temperature is, inevitably, the average translational temperature of the C_2H_2 molecules along the line of sight of the laser beam, but the line profiles are, nevertheless, found to fit well to a single Gaussian function and show no evidence of different components corresponding to distinctly different temperature regions.

The experimental configuration of the laser beam and filament is shown in the inset to Fig. 2, with the cavity axis parallel to the long axis of the filament, and line profiles similar to that shown in the figure were recorded at different distances, d, between the bottom of the filament coil and the laser beam. The FWHM values of these profiles, and thus the C_2H_2 temperature, were found to be independent of d in the range $0.5<d<15$ mm. The temperature derived is much lower than that measured from H-atom Doppler profiles (recorded using resonance-enhanced multi-photon ionisation spectroscopy) close to the filament [6] and indicates the presence of cold regions of acetylene, undoubtedly in the extremities of the reactor. A very similar observation was made in the arc-jet reactor, for which an average C_2H_2 temperature of 550 ± 200 K, irrespective of probe distance from the substrate, was measured from the Doppler-

broadened R(26) rotational line. Recent pulsed CRDS measurements of C_2 and CH radicals in this arc jet yielded $T_{gas} \approx 3200$ K in the activated region [10]. The much lower effective temperatures obtained from the present C_2H_2 measurements can be understood by recognising significant diffusion of acetylene throughout the reactor. This reflects the stability of acetylene in the production region and the fact that, away from the source of activation, there are few chemical mechanisms for its destruction. The much longer pathlength of the laser beam through the cooler regions of the reactor compared to the narrow, activated, high-temperature regions and the stability of the C_2H_2 at the lower temperatures ensure that the absorption measurements and Doppler profiles are dominated by the cooler C_2H_2. There may well be a temperature gradient within the cooler regions, giving rise to a continuous variation of Doppler broadening, but integration along the laser beam path gives a line-of-sight-averaged profile that still appears Gaussian, with a width determined by the average temperature.

3.2. Absolute concentrations

Average number densities (i.e. the number density averaged along the path of the probe beam) were calculated from spectral line intensities using the following procedure. $\Delta k_{\bar{\nu}}$ at any laser wavenumber ($\bar{\nu}$) is related to the absorption coefficient, $\alpha_{\bar{\nu}}$, at that wavenumber by:

$$\alpha_{\bar{\nu}} = \frac{\Delta k_{\bar{\nu}} \ell}{cl} \tag{2}$$

where c is the speed of light, ℓ is the mirror separation and l is the effective absorption length of the column containing C_2H_2. Since C_2H_2 is thought to diffuse throughout the reactor, ℓ and l are equal and their ratio can be neglected. Absorption cross-sections at 296 K, integrated across individual line profiles and denoted here by $\sigma_{int}(296\ \mathrm{K})$, were taken from the work of El Hachtouki and Van der Auwera [16]. For measurements at 296 K, total number densities of acetylene, $[C_2H_2]$, can be derived from absorption coefficients integrated across line profiles using:

$$[C_2H_2] = \frac{\int_{line} \alpha_{\bar{\nu}}\, d\bar{\nu}}{\sigma_{int}(296\ \mathrm{K})} \tag{3}$$

The $\sigma_{int}(T)$ values are, however, T-dependent parameters because of changing populations of the various rotational and vibrational energy levels of acetylene at different temperatures. They must, therefore, be corrected for the average temperature of 550 K before acetylene concentrations can be derived from the CRDS measurements in the arc jet and HF reactors, and this is achieved using:

$$\sigma_{int}(T) = \sigma_{int}(296\ \mathrm{K}) \frac{q_v(296\ \mathrm{K})}{q_v(T)} \frac{f_r(T)}{f_r(296\ \mathrm{K})} \tag{4}$$

where $q_v(T)$ are temperature-dependent vibrational partition functions and $f_r(T)$ is a rotational line-dependent correction factor that reflects the fraction of the total vibrational band strength that is carried by the probed rotational line at temperature T. The $f_r(T)$ factors were calculated by simulation of the entire $\nu_1 + \nu_3$ band at 296 and 550 K using PGOPHER [14] and evaluation of the fractional contribution that each recorded R(J) line makes to the total band intensity in each of the simulations. Acetylene concentrations cited hereafter and plotted in later figures were thus derived using line-integrated measured absorption coefficients via:

$$[C_2H_2] = \frac{\int_{line} \alpha_{\bar{\nu}}\, d\bar{\nu}}{\sigma_{int}(550\ \mathrm{K})} \tag{5}$$

with $\sigma_{int}(550\ \mathrm{K})$ calculated from Eq. (4), a $q_v(296\ \mathrm{K})/q_v(550\ \mathrm{K})$ ratio of 0.684 and the spectral intensity data of El Hachtouki and Van der Auwera [16].

Under standard growth conditions in the HF reactor (1% CH_4 in H_2, $p = 20$ Torr, $T_{fil} = 2150$ °C) the average acetylene number density is $(2.9 \pm 0.6) \times 10^{13}$ molecules cm^{-3} (with the uncertainty quoted reflecting the standard deviations of the fits and the outcomes of repeated measurements, but not allowing for the uncertainty in the gas temperature). This number density equates to ~1.7% of the total carbon fed in as CH_4 and compares well with our preliminary 2-D model calculations predicting $\sim 6.5 \times 10^{12}$ molecules cm^{-3}. The average number density deduced for C_2H_2 in the arc jet is $(1.2 \pm 0.2) \times 10^{14}$ molecules cm^{-3}, corresponding to some 40% of the total carbon feed. The arc jet conditions for these measurements (0.5% CH_4 in H_2 and excess Ar, 50 Torr, 5.8-kW discharge power) involved lower CH_4 flow rates than those used for optimum diamond growth (typically 60 sccm, or 3.3% of the total flow rate) since, at such high flow rates, the associated increase in acetylene saturated the ring-down signal. This observation and the deliberate use of spectroscopic transitions originating from rotational levels with unfavourable nuclear spin statistics illustrate the sensitivity of the CW-CRDS measurements. Work is in progress to formulate models of the arc jet chemistry and transport for comparison with the results for C_2H_2, but has so far concentrated on radical densities in the plume [8].

The large difference in the respective methane → acetylene conversion efficiencies in the two systems

reflects the very different volumes of, and gas temperatures in, the activated regions of the different reactors. In the HF reactor, the thermally activated chemistry is primarily confined to a small cylindrical region about the filament with length determined by the filament coil ($\sim$12 mm) and extending $\sim$15 mm radially (as established from measurements of H-atom and CH_3-radical spatial profiles) [18]. Thus, a large fraction of the flow of feed gases, introduced above the filament region, passes through the reactor to the exhaust line without sampling this volume. Conversely, in the DC arc jet, the plume volume is defined by the diameter ($\geq$12 mm) and length (typically 150 mm) of the plume, the flows of H and H_2 are largely confined to the plume by the nozzle expansion, and CH_4 addition is by expansion from a ring surrounding the plume axis to encourage CH_4 entrainment. The abundance of H atoms in the high-temperature plume also encourages rapid removal of successive hydrogen atoms from CH_4 to form a relatively high density of C atoms that react with CH to form C_2, which ultimately leads to production of C_2H_2 and higher C_xH_y ($x \geq 3$) species [8].

Spatial variations in the acetylene number density and temperature were probed in both reactors. In the case of the HF reactor, the position of the filament was moved vertically 0–15 mm from the central (horizontal) axis of the CRD spectrometer. For the arc jet, the position of the substrate was moved along the axis of the activated gas plume, while the line of intersection of the plume with the laser beam remained fixed. Substrate–laser distances of 1–10 mm were covered. In both cases, no spatial variation in C_2H_2 concentration or temperature was found. These observations should be contrasted with measurements of the spatial variation of the density and temperature of radical species (such as CH_3, NH, C_2 and CH) that we have made by pulsed laser CRDS in the same reactors [7,10], and further encourage the conclusion that acetylene is present throughout the entire volume of both chambers, whereas the radicals are localised in the activated regions.

3.3. The effects of reactor operating parameters

Two operating parameters of the reactors that can be straightforwardly varied to learn more about the activation and chemistry of the gas-phase component of the CVD process are the percentage of methane in the feedstock gas and the input power. In the hot-filament reactor, increased input power causes a rise in the temperature of the filament and thus promotes dissociation of H_2 to H atoms. In the DC arc jet, an increase in the power (by increasing the voltage and/or current supplied to the discharge) likewise encourages greater thermal dissociation of H_2 [8].

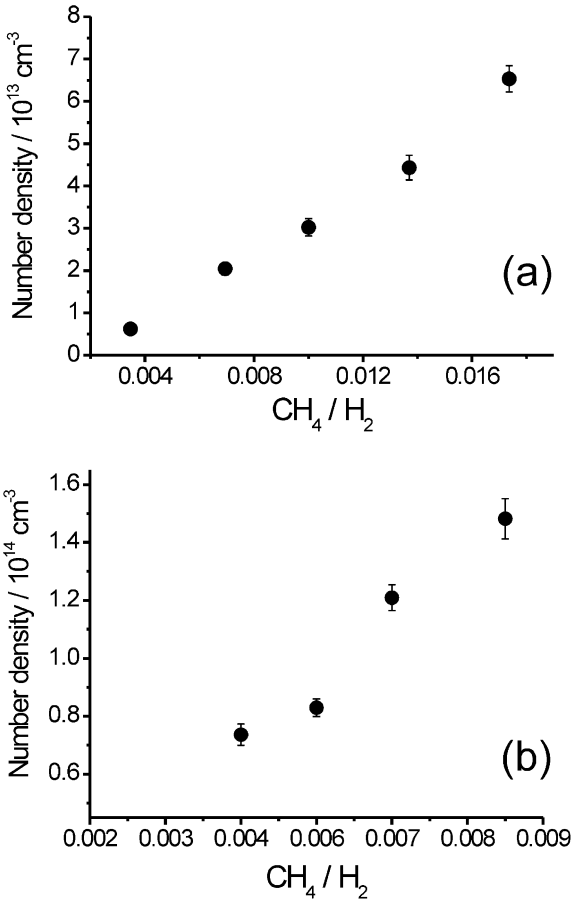

Fig. 3. Variation of the acetylene number density with increasing CH_4 fraction in the feed gas in (a) the HF reactor (with T_{fil} = 2150 °C, p = 20 Torr and d = 3 mm) and (b) the arc jet reactor (input power 5.8 kW, p = 50 Torr). Number density values were derived from integrated absorption values of the R(22) (HF reactor) and R(26) (arc jet) lines of the C_2H_2 $\nu_1+\nu_3$ band.

3.3.1. Feed-gas methane fraction

In the HF reactor, full absorption profiles of the R(22) line of the $\nu_1+\nu_3$ acetylene combination band were scanned for various CH_4/H_2 input ratios ranging from 0.3 to 1.8%. At higher methane levels, so much of the laser beam was absorbed that ring-down measurements became impossible using this spectroscopic line. Integration of line intensities and conversion to C_2H_2 number densities, using the procedure described above and assuming that acetylene fills the entire distance between the mirrors, gave the data plotted in Fig. 3a. As is evident from the figure, there is a near-linear increase in C_2H_2 number density with fraction of added methane.

Similar measurements using the R(26) acetylene absorption line were repeated in the DC arc jet reactor for CH_4 flows from 8 to 15 sccm (i.e. CH_4/H_2 ratios of 0.4–0.8%), and an equivalent analysis yielded the data plotted in Fig. 3b. Again, there is a monotonic rise in the concentration of C_2H_2 as the fraction of added methane is increased. Methane flows greater than 15

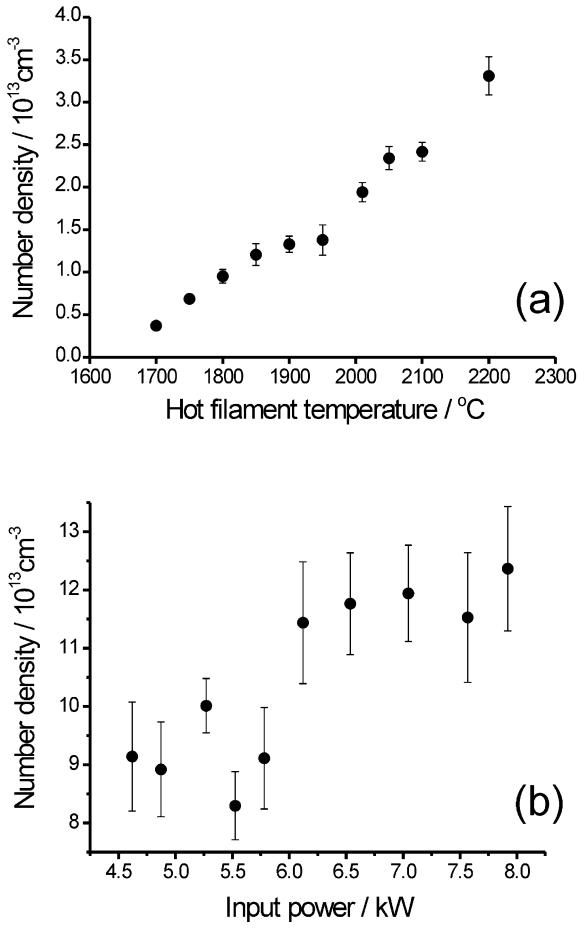

Fig. 4. The dependence of acetylene number density on (a) the temperature of the filament in the HF reactor (for 1% CH_4/H_2, $d=3$ mm and $p=20$ Torr) and (b) the discharge power in the arc jet reactor (for 0.5% CH_4/H_2 and $p=50$ Torr). Number density values were derived from analysis of the same spectral lines as in Fig. 3.

sccm resulted in C_2H_2 absorption too strong for the CRDS measurements on the R(26) line. Clearly, higher C_2H_2 concentrations could be measured using lines with lower linestrength or levels with smaller relative rovibrational population, but restrictions of stable operation of the diode laser at other wavelengths have so far prevented these measurements.

3.3.2. Input power

The input power to the HF reactor is controlled by current and voltage settings for the electrical supply to the filament. The temperature of the filament, as measured with a pyrometer, can consequently be varied, and Fig. 4a shows the pronounced dependence of the C_2H_2 number density [from integrated intensities of the R(22) rotational line] on the filament temperature, for otherwise standard operating conditions of 1% CH_4 in H_2 at a total pressure of 20 Torr. Analysis of the widths of the Doppler-broadened spectral lines, however, shows no variation about a mean C_2H_2 temperature of ~550 K, despite variation of the filament temperature from 1700 to 2200 °C.

The quality of data obtained from power-dependent studies in the DC arc jet was lower, because of instabilities in its operation over the timescale of the measurements, but the variation in C_2H_2 concentration with input power ranging from 4.6 to 8.0 kW at a methane flow of 10 sccm (0.5% CH_4/H_2), as shown in Fig. 4b, illustrates a weak trend to greater C_2H_2 production at higher arc jet powers. As was observed for the HF reactor, however, the Doppler widths of the acetylene absorption lines show no discernible variation with input power, and exhibit a mean temperature of ~550 K.

A full interpretation of the dependence of C_2H_2 concentration on the operating parameters of gas mixture and input power as measured must await implementation of numerical models of C_2H_2 production in the two reactors, but some qualitative observations are pertinent. Increasing CH_4 fraction unsurprisingly results in greater formation of C_2H_2, because this latter molecule acts as a carbon reservoir with low reactivity. All the carbon-containing chemistry leading to C_2H_2 formation is promoted by increased methane inputs. Likewise, increased filament temperature or arc-jet discharge power promotes H atom formation that drives the gas-phase chemistry towards C_2H_2 production, although in the arc jet a near-doubling of the input power gives only an approximately 30% increase in the concentration of C_2H_2. The insensitivity of the C_2H_2 temperatures measured to input power (either filament temperature or arc jet discharge power) supports the assertion that C_2H_2 is widely distributed in the reactor and that we therefore measure an average temperature sampled through the changing activated region and the larger, but invariant and cooler, surrounding stagnant volumes.

3.4. Acetylene diffusion times

The CRDS measurements establish that acetylene is present in the colder regions of the reactor at equilibrium, but it is mostly created in the central, activated region, and hence takes time to diffuse outwards. It is also continuously removed by pumping of the reactor volume to maintain the flow rate at 100 sccm at pressure of 20 Torr in the HF reactor or ~14 slm and 50 Torr in the arc jet reactor. The timescales for these production, diffusion and pump-out processes are measurable using the existing apparatus.

Measurements of the build-up of acetylene in the HF reactor after its production is initiated and its decay when production is halted have been made by following the temporal behaviour of the C_2H_2 signal after switching on or off the current to the HF. These experiments were repeated at different chamber pressures and flow rates. To facilitate continuous measurement, the probe wavelength was positioned at the centre of the R(22)

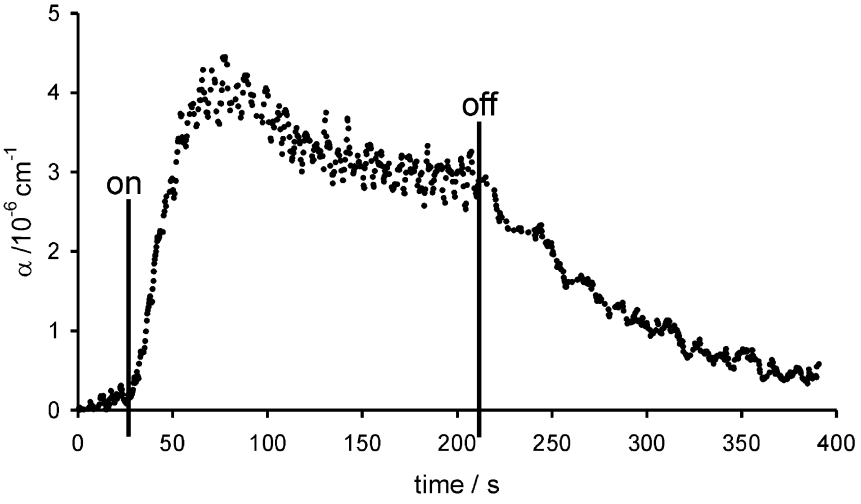

Fig. 5. Time-dependent build-up and decay of acetylene in the HF reactor (1% CH_4/H_2, $T_{fil}=2150$ °C) after HF switch on/off. The data points plotted are line-centre absorption coefficients derived from changes in the ring-down time for a laser frequency set at the centre of the R(22) line of the C_2H_2 $\nu_1+\nu_3$ band. The vertical bars indicate the times at which the hot filament was switched on and off.

absorption line and held constant while successive ring-down measurements were made, and the line-centre absorption coefficient values derived plotted against time. Fig. 5 shows typical growth and decay of the C_2H_2 signal with time in the HF reactor.

3.4.1. Time-dependent behaviour of the C_2H_2 signal in the HF reactor

Fig. 5 shows a rapid increase in C_2H_2 absorbance over the first minute after switch-on of a pre-carburised filament operating in a 1% CH_4/H_2 gas mixture, reaching a peak at $\alpha=4\times10^{-6}$ cm^{-1}, which then decays over the next 2 min to a constant level of $\alpha=3\times10^{-6}$ cm^{-1}. The length of time for build-up is in part a consequence of the time required for acetylene to diffuse into the cold regions after production near the filament. Changes in the temperature of the gas, and hence in the Boltzmann population of the rotational level probed, will also affect the measured signals, but to a lesser extent than diffusion. The growth of C_2H_2 is well modelled by an exponential function:

$$[C_2H_2]\approx[C_2H_2]_\infty\left(1-\exp\left(-(t-t_{on})/\tau_+\right)\right) \quad (6)$$

where $[C_2H_2]_\infty$ is the asymptotic acetylene number density under stable operating conditions of the reactor, $(t-t_{on})$ is the time since switch-on of the HF, and τ_+ is the rise time constant.

Similarly, after switch-off the decaying signal is well fitted by:

$$[C_2H_2]\approx[C_2H_2]_\infty\left(1-\exp\left(-(t-t_{off})/\tau_-\right)\right) \quad (7)$$

where t_{off} is the time at which the filament is extinguished and τ_- is the decay time constant. Tables 1 and 2 summarise the τ_+ and τ_- values measured under different conditions of flow rate and pressure from fits to curves such as that shown in Fig. 5.

The time for slow, diffusional filling of cold, cylindrical, stagnant regions at a distance L from the source of C_2H_2 may be estimated as [19]:

$$\tau_{diff}\approx\frac{4L^2}{\pi^2 D} \quad (8)$$

Table 1
Time constants measured for the growth and decay of C_2H_2 absorbance in a HF reactor at constant pressure for different feed gas flow rates, together with the diffusion (τ_{diff}) and residence (τ_r) times calculated within the reactor ($p=20$ Torr, 1% CH_4 in H_2, $T_{fil}=2150$ °C)

Flow rate (sccm)	τ_+ (s)	τ_{diff} (s)	τ_- (s)	τ_r (s)
50	16±1	11	200	220
100	16±1	11	90	110
200	16±1	11	70±5	55

Error estimates represent reproducibility ranges for the values from different experiments.

Table 2
Time constants measured for the growth and decay of C_2H_2 absorbance in a HF reactor at constant flow rate for varying reactor pressures, together with the timescale calculated for diffusion (τ_{diff}) and residence (τ_r) times within the reactor (flow rate 100 sccm, 1% CH_4 in H_2, $T_{fil}=2150$ °C). Error estimates represent reproducibility ranges of the values from different experiments.

Pressure (Torr)	τ_+ (s)	τ_{diff} (s)	τ_- (s)	τ_r (s)
10	6±1.5	6.6	35±5	55
20	14±1	11	90	110
40	20±1	22	200	220

The diffusion coefficient, D, for C_2H_2 in H_2 was taken as follows [20,21]:

$$D = 0.125 \times \frac{T^{1.5}}{p} \quad (9)$$

Two-dimensional calculations show that the limiting rate for the present experimental conditions ($L = 30$ cm, $p = 20$ Torr) is associated with diffusional filling of the most distant stagnant regions, wherein the gas temperatures are close to $T_{wall} \approx 300$ K. Under such conditions, Eqs. (8) and (9) yield $D = 32.5$ cm^2 s^{-1} and $\tau_{diff} = 11$ s. Corresponding values for the other experimental pressures are displayed in Table 2. Estimates of the rates of convective transport of C_2H_2 into the stagnant regions show the timescales to be much slower (by approximately one order of magnitude) than diffusional transfer.

After filament switch-off and the ensuing rapid gas cooling, there are no significant gas-temperature and species-density gradients in the whole reactor volume. The removal time (τ_-) for acetylene after the HF is extinguished is therefore well approximated by the residence time in the reaction vessel, which is the average time that a gas molecule spends within the vacuum chamber. The residence time τ_r for a particle within a continuously pumped and replenished system of volume V is given by L/v where v is the flow velocity, and can be rewritten as:

$$\tau_r = 79.05 \times \frac{pV}{Q} \quad (10)$$

where Q is the flow rate in sccm, p is in Torr and V is in litres. The equation is valid if all species are removed equally efficiently, and the residence times calculated are listed in Tables 1 and 2.

The calculated diffusion and removal timescales given in Tables 1 and 2 fit well with the experimental observations, suggesting that the temporal variation in absorbance shown in Fig. 5 is determined by diffusion and pump-out. This analysis does not, however, account for the peak in the acetylene absorption shortly after switch-on of the filament in the HF reactor. We considered two possible explanations for such behaviour. The first is that the peak is a natural feature of the gas-phase chemistry. Although our modelling studies do indeed predict peaks in the temperature-dependent (and thus time-dependent) production rate of many hydrocarbon species, including C_2H_2, the relevant timescales are typically of the order of a few seconds, and do not appear to account for the much slower peaking (over at least 60 s) observed in the HF reactor. Our preferred explanation has a simpler, physical origin. When the filament is first switched on, the HF temperature (T_{fil}) is set to 2150 °C, but, as the filament and the immediate surrounding gas heat up, the filament power has to be gradually reduced over a period of 3–5 min in order to maintain a constant temperature (as measured with the pyrometer), after which the power and T_{fil} remain stable. This suggests some change in filament efficiency during the initial period. A conditioned Ta filament as used here (i.e. one that has already been run in the presence of C for several hours) is envisaged to be mainly TaC, with a surface that is partially shrouded by a coating of graphitic carbon. It is likely that during the initial thermal shock of filament switch-on, some fracturing of the filament surface may occur due to differing rates of expansion of the TaC filament core and the graphitic surface. These fractures will have the effect of increasing the filament surface area and exposing more TaC, both of which will increase the filament efficiency for H_2 dissociation. After some time, the cracks will be recovered with a graphitic coating. Graphitic surfaces are known to catalyse H_2 dissociation less efficiently than a 'clean' TaC surface [22,23]. In this scenario, the H_2 dissociation efficiency of the filament should fall during this period, as should the H atom production rate, and thus the steady-state concentration of acetylene within the chamber. Such expectations accord with experimental observations, and suggest timescales for re-graphitisation very comparable to those deduced for N-substitution of a graphitised TaC surface upon addition of NH_3 to an HF-activated CH_4/H_2 gas mixture [7].

3.4.2. Time-dependent behaviour of the C_2H_2 signal in the DC arc jet reactor

Precise studies of the time dependence of acetylene absorption in the arc jet are more difficult to perform than in the HF reactor because the start-up procedure of the arc jet discharge is much more complicated than simple switch-on of current to the hot filament. The most straightforward way to measure build-up and decay of the absorption is to start and stop the flow of methane to the gas plume using a valve located in the methane supply line, upstream of the ring that injects the methane into the reactor. This procedure has an associated delay in the control of methane delivery to the arc jet plume of only ~ 1 s, so on- and off-times for C_2H_2 production are sufficiently well defined to study its build-up and loss. Experiments were performed in which the absorption at the peak of the R(30) rotational line of the C_2H_2 $\nu_1 + \nu_3$ combination band was monitored as methane flow was initiated, allowed to run for times of the order of a few minutes, and then terminated. Before starting the methane flow, all other operating parameters of the arc jet were set to their usual values, i.e. the plasma torch was running stably with a mixture of H_2 and excess Ar at discharge power of 7 kW. Fig. 6 shows the outcomes of the measurements obtained following the start of 15 sccm of CH_4 and its termination. The

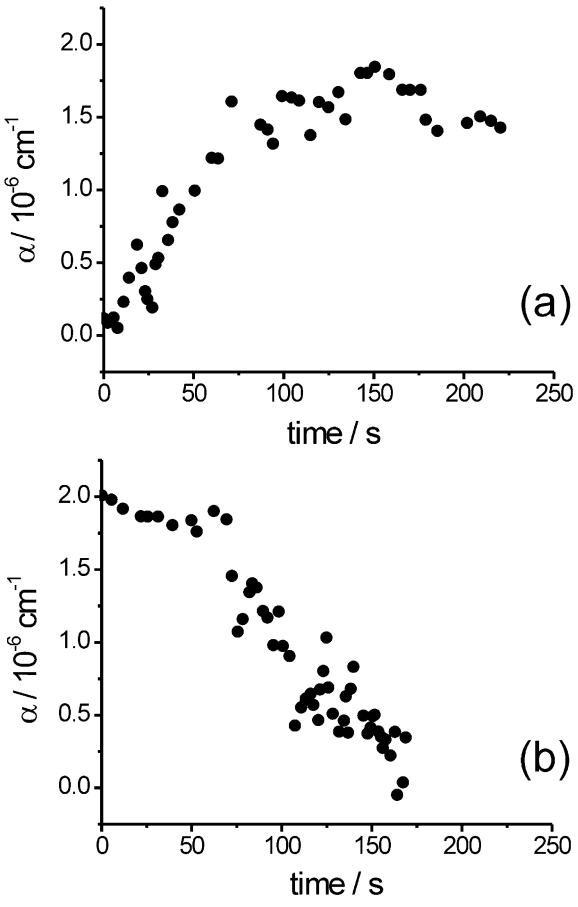

Fig. 6. Time-dependent (a) build-up and (b) decay of acetylene in the DC arc jet reactor after initiation and termination of the CH_4 flow. As in Fig. 5, the data points plotted are line-centre absorption coefficients, but were measured for the R(30) line of the C_2H_2 $\nu_1+\nu_3$ band. Data were recorded for a substrate–laser beam distance of 20 mm, CH_4 flow of 15 sccm (i.e. a CH_4/H_2 ratio of 0.8%) and discharge power of 7 kW.

distance of the substrate from the laser axis was 20 mm, so experiments probe the free plume region of the plasma jet.

The build-up and decay of the C_2H_2 absorption occur on similar timescales to those in the HF reactor, and thus are likely to be caused by C_2H_2 formation within, or in close proximity to, the activated plume, followed by diffusion to the cooler regions of the vacuum chamber and pump-out. There is no evidence for an early maximum in the build-up of absorption of the type observed in the HF reactor.

4. Conclusions

The effectiveness of diode laser cavity ring-down spectroscopy as a diagnostic tool for technological plasmas has been shown through measurements in two extremely luminous environments. The compact nature of the laser and other optics, coupled with the use of fibre optics, gives this spectrometer design great potential in the field of plasma diagnostics for systems under analysis that cannot be reached with, or are perturbed by, alternative, more invasive sampling methods. Quantitative CRDS measurements of absolute acetylene concentrations and temperatures in HF and DC arc plasma-jet diamond CVD reactors operating with CH_4/H_2 input gas mixtures allow respective estimates of 1.7 and 40% conversion of the total carbon budget into C_2H_2. The very different conversion efficiencies of the reactors reflect the different volumes of activated gases in the two CVD environments, the ways in which feedgas flows are delivered to the activated regions, and the extent of production of C_1 and C_2 radicals from the feedstock CH_4. They parallel the relative growth rates of diamond films in the HF and DC arc jet reactors ($\sim$1 and 100 μm h^{-1}, respectively, under normal operating conditions). The C_2H_2 concentrations measured ($2.9\pm0.6\times10^{13}$ and $1.2\pm0.2\times10^{14}$ molecules cm^{-3} in the HF and DC arc jet reactors, respectively) also provide critical tests of computer models of the activation, chemical mechanisms and gas transport in the reactors. Preliminary two-dimensional models of the HF reactor predict C_2H_2 concentrations within a factor of five of those measured.

Variations in C_2H_2 concentration with time from switch-on or -off of the reactors demonstrate diffusion of acetylene produced in the hot, activated regions to the cold, stagnant regions of the reaction vessels, where it remains at an equilibrium concentration until being lost at a pump-out-limited rate when production is halted. Some of the C_2H_2 thus accumulated in the cooler regions of the reactor is inevitably transported back into the activated region and acts as another carbon radical source. The CRDS measurements thus demonstrate the importance of inclusion of this additional carbon reservoir and source in any complete three-dimensional modelling of the gas-phase chemistry occurring in diamond CVD reactors.

Acknowledgments

We are grateful to De Beers Industrial Diamonds (now Element Six Ltd) for the loan of the DC-arc plasma jet system, the EPSRC for equipment funding (via the Technological Plasmas Initiative), a senior research fellowship (MNRA) and project studentship (JBW), and the Royal Society for support for the Bristol–Moscow collaboration. We also thank K.N. Rosser and Dr J.A. Smith for their many important contributions to this work.

References

[1] J.E. Field (Ed.), The Properties of Natural and Synthetic Diamond, Academic Press, London, 1992, p. 710.

[2] B. Dischler, C. Wild (Eds.), Low-Pressure Synthetic Diamond, Springer-Verlag, Berlin, 1998, p. 384.
[3] D.G. Goodwin, J.E. Butler, in: M.A. Prelas, O. Popovici, L.K. Bigelow (Eds.), Handbook of Industrial Diamonds and Diamond Films, Marcel Dekker, New York, 1998, pp. 527–580.
[4] C.A. Rego, P.W. May, C.R. Henderson, M.N.R. Ashfold, K.N. Rosser, N.M. Everitt, Diamond Relat. Mater. 4 (1995) 770.
[5] Y.A. Mankelevich, N.V. Suetin, M.N.R. Ashfold, J.A. Smith, E. Cameron, Diamond Relat. Mater. 10 (2001) 364.
[6] M.N.R. Ashfold, P.W. May, J.R. Petherbridge, et al., Phys. Chem. Chem. Phys. 3 (2001) 3471.
[7] J.A. Smith, J.B. Wills, H.S. Moores, et al., J. Appl. Phys. 92 (2002) 672.
[8] Y.A. Mankelevich, N.V. Suetin, M.N.R. Ashfold, et al., Diamond. Relat. Mater., in press.
[9] S.A. Redman, C. Chung, K.N. Rosser, M.N.R. Ashfold, Phys. Chem. Chem. Phys. 1 (1999) 1415.
[10] J.B. Wills, J.A. Smith, W.E. Boxford, J.M.F. Elks, M.N.R. Ashfold, A.J. Orr-Ewing, J. Appl. Phys. 92 (2002) 4213.
[11] D. Romanini, A.A. Kachanov, N. Sadeghi, F. Stoeckel, Chem. Phys. Lett. 264 (1997) 316.
[12] K.J. Schulz, W.R. Simpson, Chem. Phys. Lett. 297 (1998) 523.
[13] M.D. Wheeler, S.M. Newman, A.J. Orr-Ewing, M.N.R. Ashfold, J. Chem. Soc. Faraday Trans. 94 (1998) 337.
[14] M.E. Green, C.M. Western, J. Chem. Phys. 104 (1996) 848, summary of the program and Hamiltonian used for the PGOPHER spectral simulation program written by C.M. Western.
[15] B.C. Smith, J.S. Winn, J. Chem. Phys. 89 (1988) 4638.
[16] R. El Hachtouki, J. Van der Auwera, J. Mol. Spectrosc. 216 (2002) 355.
[17] F. Herregodts, D. Hurtmans, J. Van der Auwera, M. Herman, Chem. Phys. Lett. 316 (2000) 460.
[18] J.A. Smith, M.A. Cook, S.R. Langford, S.A. Redman, M.N.R. Ashfold, Thin Solid Films 368 (2000) 169.
[19] Y.P. Raizer, Physics of a Gas Discharge, Nauka, Moscow, 1987, p. 159, (in Russian).
[20] I.S. Grigoriev, E.Z. Meilichov (Eds.), Physical Values Handbook, Energoatomizdat, Moscow, 1991 (in Russian).
[21] T. DebRoy, K. Tankala, W.A. Yarbrough, R. Messier, J. Appl. Phys. 68 (1990) 2424.
[22] D. Morel, W. Hänni, Diamond Relat. Mater. 7 (1998) 826.
[23] D.M. Li, R. Hernberg, T. Mäntylä, Diamond Relat. Mater. 7 (1998) 1709.